CMS Physics Analysis Summary

Contact: cms-pag-conveners-susy@cern.ch 2017/03/22

Search for supersymmetry in pp collisions at $\sqrt{s} = 13$ TeV in the single-lepton final state using the sum of masses of large-radius jets

The CMS Collaboration

Abstract

Results are reported from a search for supersymmetric particles in proton-proton collisions in the final state with a single high transverse momentum lepton; multiple jets, including at least one b-tagged jet; and large missing transverse momentum. The search uses a 35.9 fb^{-1} sample of proton-proton collision data at $\sqrt{s} = 13$ TeV accumulated by the CMS experiment at the LHC. The observed event yields in the signal regions are consistent with those expected for standard model backgrounds. The results are interpreted in the context of simplified models of supersymmetry involving gluino pair production, with gluino decay into either on- or off-mass-shell top squarks. Assuming that the top squarks decay into a top quark plus a stable, weakly interacting neutralino, scenarios with gluino masses up to about 1.9 TeV are excluded at a 95% CL for neutralino masses up to about 1 TeV.

A central goal of the physics program of the CMS experiment at the CERN Large Hadron Collider is the search for new particles and phenomena beyond the standard model (SM), in particular supersymmetry (SUSY) [1–8]. During 2016, CMS accumulated a data sample of proton-proton collisions at center-of-mass energy 13 TeV corresponding to 35.9 fb^{-1}, significantly extending the sensitivity to the production of new heavy particles. The search described here focuses on a generically important experimental signature that is also strongly motivated by SUSY phenomenology. This signature includes a single lepton (an electron or muon); several jets, corresponding to energetic quarks and gluons; at least one b-tagged jet, indicative of processes coupling to third generation quarks; and finally, missing momentum, $\vec{p}_{\mathrm{T}}^{\mathrm{miss}}$, in the direction transverse to the beam. A large value of $p_{\mathrm{T}}^{\mathrm{miss}} \equiv |\vec{p}_{\mathrm{T}}^{\mathrm{miss}}|$ can arise from the production of high momentum, weakly interacting particles that escape detection. Searches for SUSY in the single-lepton final-state have been performed both by ATLAS and CMS at 8 TeV [9, 10] and 13 TeV [11–13]. The present analysis is based largely on methodologies described in detail in Ref. [12], which include the use of large radius jets and related kinematic variables.

In models based on SUSY, new particles are introduced such that all fermionic (bosonic) degrees of freedom in the SM are paired with corresponding bosonic (fermonic) degrees of freedom in the extended theory. The discovery of a Higgs boson with low mass [14–19] provides a key motivation for SUSY. Stabilizing the Higgs boson mass at a low value, without invoking extreme fine tuning of parameters, is a major theoretical challenge, referred to as the gauge hierarchy problem [20–25]. This stabilization can be achieved in so-called natural SUSY models [26–29], in which several of the SUSY partners are constrained to be light [28]: the top squarks, $\widetilde{\mathrm{t}}_L$ and $\widetilde{\mathrm{t}}_R$, which have the same electroweak couplings as the left- (L) and right- (R) handed top quarks, respectively; the bottom squark with L-handed couplings ($\widetilde{\mathrm{b}}_L$); the gluino ($\widetilde{\mathrm{g}}$); and the Higgsinos ($\widetilde{\mathrm{H}}$). This search targets gluino pair production, which has a relatively large cross section process for a given mass, with gluino decay $\widetilde{\mathrm{g}} \to \mathrm{t\bar{t}}\tilde{\chi}_1^0$. This process can arise from $\widetilde{\mathrm{g}} \to \widetilde{\mathrm{t}}_1\bar{\mathrm{t}}$, where the top squark is produced either on or off mass shell. The symbol $\tilde{\chi}_1^0$ denotes the lightest neutralino, a neutral mass eigenstate that is in general a mixture of the higgsinos and gauginos. In R-parity conserving SUSY models [30, 31] in which the $\tilde{\chi}_1^0$ is the lightest supersymmetric partner (LSP), the $\tilde{\chi}_1^0$ is stable and can, in principle, account for some or all of the astrophysical dark matter. The scenario with off-mass-shell top squarks is denoted as T1tttt [32] in simplified model scenarios [33–35]. In natural SUSY models, the mass of the top squark is typically constrained to be lighter than that of the gluino, so we also search for scenarios with on-shell top squarks, denoted as T5tttt.

The central feature of the CMS detector is a superconducting solenoid of 6 m internal diameter, providing a magnetic field of 3.8 T. Within the solenoid volume are the charged particle tracking systems, composed of silicon-pixel and silicon-strip detectors, and the calorimeter systems, consisting of a lead tungstate crystal electromagnetic calorimeter (ECAL) and a brass and scintillator hadron calorimeter (HCAL). Muons are identified and measured by gas-ionization detectors embedded in the magnetic flux-return yoke outside the solenoid. A more detailed description of the CMS detector, together with a definition of the coordinate system used and the relevant kinematic variables, is given in Ref. [36].

Simulated event samples for SM background processes are used in the design of the event selection and to determine correction factors, typically near unity, that are used in conjunction with observed event yields in control regions to determine the SM background contribution in the signal regions. The production of $\mathrm{t\bar{t}}$+jets, W+jets, Z+jets, and QCD multijet events is simulated with the Monte Carlo (MC) generator MADGRAPH5_aMC@NLO 2.2.2 [37] in leading-order (LO) mode. Details on the simulated event samples for SM backgrounds, including the parton distribution functions, parton showering, the underlying event model and cross sections used, and other processes with smaller contributions (single-top, $\mathrm{t\bar{t}}$+bosons, diboson, and $\mathrm{t\bar{t}t\bar{t}}$ production) are given in Ref. [12]. The detector simulation is performed with GEANT4 [38]. Simulated event samples for SUSY signal models are used to determine the detector acceptance and event selection efficiency for signal events. Signal events for the T1tttt and T5tttt simplified models are generated in a manner similar to that used for the SM backgrounds. Because of the large number of mass hypotheses scanned over to obtain results for these models, however, the detector simulation in this case is performed with the CMS fast simulation package [39]. Scale factors are applied to account for any differences with respect to the full simulation used for SM backgrounds.

Two T1tttt benchmark models are used to illustrate typical signal behavior. The T1tttt(1800,100) model, with masses $m_{\tilde{g}} = 1800$ GeV and $m_{\tilde{\chi}_1^0} = 100$ GeV and cross section of 2.8 fb, corresponds to a scenario with a large mass splitting between the gluino and the neutralino. The T1tttt(1400,1000) model, with masses $m_{\tilde{g}} = 1400$ GeV and $m_{\tilde{\chi}_1^0} = 1000$ GeV and cross section of 25 fb, corresponds to a scenario with a small mass splitting between the gluino and the neutralino.

The data were recorded using the logical OR of several triggers, which require either a large $p_{\mathrm{T}}^{\mathrm{miss}}$, or require a single lepton (an electron or muon), both with and without a large value of H_{T}, the scalar sum of the jet transverse momenta in the event. In the region with the greatest signal sensitivity, $p_{\mathrm{T}}^{\mathrm{miss}} > 300$ GeV, triggers using $p_{\mathrm{T}}^{\mathrm{miss}}$ without any lepton requirements are fully efficient. For $200 < p_{\mathrm{T}}^{\mathrm{miss}} < 300$ GeV, the triggers based on $p_{\mathrm{T}}^{\mathrm{miss}}$ have not reached plateau efficiency, but the leptonic triggers bring the efficiency to nearly 100%.

Reconstruction proceeds from particles identified by the particle-flow (PF) algorithm [40, 41], which uses information from the tracker, calorimeters, and muon systems to identify the particle candidates as electrons, muons, charged or neutral hadrons, or photons. Electrons are reconstructed by associating a charged particle track with an ECAL supercluster [42]. The resulting candidate electrons are required to have $p_{\mathrm{T}} > 20$ GeV and pseudorapidity $|\eta| < 2.5$, and to satisfy identification criteria designed to remove light-parton jets, photon conversions, and electrons from heavy flavor hadron decays. Muons are reconstructed by associating tracks in the muon system with those found in the silicon tracker [43]. Muon candidates are required to satisfy $p_{\mathrm{T}} > 20$ GeV and $|\eta| < 2.4$. To select leptons from W-boson decay, leptons are required to be isolated from other PF candidates. Isolation is quantified using an optimized version [12] of the mini-isolation variable originally suggested in Ref. [44], in which the transverse energy of the particles within a cone in η-ϕ space surrounding the lepton momentum vector is computed using a cone size that scales as $1/p_{\mathrm{T}}^{\ell}$, where $\vec{p}_T^{\ell}$ is the transverse momentum of the lepton.

The dominant background in the analysis arises from $\mathrm{t\bar{t}}$ dilepton events in which one of the leptons is not reconstructed, fails the lepton selection criteria (including isolation), or is a τ lepton decaying to hadrons. To further suppress the dilepton $\mathrm{t\bar{t}}$ background, we veto events that contain a broader category of candidates for the second lepton, referred to as veto tracks. These include two categories of charged tracks: isolated leptons satisfying looser identification criteria than lepton candidates, including a lowered momentum requirement, $p_{\mathrm{T}} > 10$ GeV, and isolated hadronic PF candidates, which must satisfy $p_{\mathrm{T}} > 15$ GeV. In either case, the charge of the veto track must be opposite to that of the lepton candidate in the event. To maintain high efficiency for signal events, lepton veto tracks must satisfy a requirement on the stransverse mass quantity [45] $M_{\mathrm{T2}}(\ell^{\pm}, v^{\mp}, \vec{p}_{\mathrm{T}}^{\mathrm{miss}}) < 80$ GeV and hadronic veto tracks must satisfy $M_{\mathrm{T2}}(\ell^{\pm}, v^{\mp}, \vec{p}_{\mathrm{T}}^{\mathrm{miss}}) < 60$ GeV, where $\ell^{\pm}$ is the candidate signal lepton and $v^{\mp}$ is the oppositely charged veto track.

Charged PF candidates and the neutral PF candidates are clustered into jets using the anti-k_{T}

algorithm [46] with distance parameter $R = 0.4$, as implemented in the FASTJET package [47]. Jets are required to satisfy $p_T > 30$ GeV and $|\eta| \leq 2.4$. Additional details and references are given in Ref. [12] on the p_T- and η-dependent jet-energy calibration, the jet identification requirements, and the subtraction of the energy contribution to the jet p_T from multiple proton-proton interactions from the same or neighboring beam crossings (pileup).

A subset of the jets are "tagged" as originating from b quarks using the combined secondary vertex (CSV) algorithm [48, 49]. For the working point used here, the signal efficiency for b jets in the range $p_T = 30$ to 80 GeV is 60–67% (51–57%) in the barrel (endcap), increasing with p_T. The misidentification probability for c quarks is roughly 13%, while that for light flavor quarks or gluinos is 1–2%.

We cluster the jets with $R = 0.4$ (small-R jets) and the isolated leptons into $R = 1.4$ (large-R) jets using the anti-k_T algorithm. The masses of the large-R jets reflect the p_T spectrum and multiplicity of the clustered objects, as well as their angular spread. The variable M_J is defined as the sum of all large-R jet masses: $M_J = \sum_{J_i=\text{large-}R\text{ jets}} m(J_i)$. For $\mathrm{t\bar{t}}$ events with a small contribution from initial-state radiation (ISR), the M_J distribution has an approximate cutoff at $2m_t$. In contrast, the M_J distribution for signal events extends to larger values. The presence of a significant amount of ISR generates a high-M_J tail in the $\mathrm{t\bar{t}}$ background, producing the main source of background in the analysis.

The missing transverse momentum, p_T^{miss}, is defined as the magnitude of $\vec{p}_T^{miss}$, the negative vector sum of the transverse momenta of all PF candidates [40, 41]. To separate backgrounds characterized by the presence of a single W boson decaying leptonically, but without any other source of missing momentum, we use the transverse mass $m_T = \sqrt{2 p_T^{\ell} p_T^{miss} [1 - \cos(\Delta\phi_{\ell,\vec{p}_T^{miss}})]}$, where $\Delta\phi_{\ell,\vec{p}_T^{miss}}$ is the difference between the azimuthal angles of $\vec{p}_T^{\,\ell}$ and $\vec{p}_T^{miss}$. The quantity H_T is defined as the scalar sum of the transverse momenta of all the small-R jets passing the selection, while $S_T = H_T + p_T^{\ell}$.

We select events with exactly one isolated charged lepton (an electron or a muon), no veto tracks, $S_T > 500$ GeV, $p_T^{miss} > 200$ GeV, and at least six small-R jets, at least one of which is b tagged. After this set of requirements, referred to in the following as the *baseline selection*, about 80% of the SM background arises from $\mathrm{t\bar{t}}$ production. The contributions from events with a single top quark or a W boson in association with jets are each about 6–8%; much of the remainder is from events with $\mathrm{t\bar{t}}$ produced in association with a vector boson. The background from QCD multijet events after the baseline selection is negligible.

The analysis is performed by defining four regions in the M_J-m_T plane: three control regions (CR) and one signal region (SR):

- R1 (CR): $m_T \leq 140$ GeV, $250 \leq M_J \leq 400$ GeV,
- R2 (CR): $m_T \leq 140$ GeV, $M_J > 400$ GeV,
- R3 (CR): $m_T > 140$ GeV, $250 \leq M_J \leq 400$ GeV, and
- R4 (SR): $m_T > 140$ GeV, $M_J > 400$ GeV.

Regions R2 and R4, which have high m_T, are subdivided into bins of p_T^{miss}, the number of small-R jets (N_{jets}), and the number of b-tagged jets (N_b) as follows:

- three p_T^{miss} bins: 200 GeV $< p_T^{miss} \leq$ 350 GeV, 350 GeV $< p_T^{miss} \leq$ 500 GeV, $p_T^{miss} >$ 500 GeV,
- two N_{jets} bins: $6 \leq N_{jets} \leq 8$, $N_{jets} \geq 9$, and

- three N_b bins: $N_\mathrm{b} = 1$, $N_\mathrm{b} = 2$, $N_\mathrm{b} \geq 3$,

giving a total of 18 bins. Backgrounds with a single W boson decaying leptonically are strongly suppressed by the requirement $m_\mathrm{T} > 140$ GeV, so the background in R3 and R4 is dominated by dilepton $\mathrm{t\bar{t}}$ events. Approximately half of the dilepton background in R4 involves a missed electron or muon and half a hadronically decaying τ lepton. Given that the main background processes have two or fewer b quarks, the total SM contribution to the $N_\mathrm{b} \geq 3$ bins is very small and is driven by the b-tag fake rate. Signal events in the T1tttt and T5tttt models populate primarily the bins with $N_\mathrm{b} \geq 2$.

The method for predicting the background yields takes advantage of the near absence of correlation between the M_J and m_T distributions in R1–R4, which is a consequence of the high jet multiplicity requirement [12]. To satisfy this requirement, background events must typically contain additional jets from ISR. Even though the background at low m_T arises largely from single-lepton $\mathrm{t\bar{t}}$ events, while the background at high m_T is dominated by dilepton $\mathrm{t\bar{t}}$ events, the presence of ISR jets results in a convergence of the M_J distributions at low and high m_T. We therefore measure the shape of the M_J distribution of the background at low m_T (R1, R2) and extrapolate it to high m_T to obtain the background prediction in R4. The mean background yields in R1–R4 are thus related by the constraint $\mu^\mathrm{bkg}_\mathrm{R4} = \kappa \cdot \mu^\mathrm{bkg}_\mathrm{R3} \cdot \mu^\mathrm{bkg}_\mathrm{R2} / \mu^\mathrm{bkg}_\mathrm{R1}$, where κ is a near-unity correction factor obtained from MC simulation of the total background:

$$\kappa = \frac{\mu^\text{MC bkg.}_\mathrm{R4} / \mu^\text{MC bkg.}_\mathrm{R2}}{\mu^\text{MC bkg.}_\mathrm{R3} / \mu^\text{MC bkg.}_\mathrm{R1}}. \tag{1}$$

This constraint is imposed by relating the expected yields in R1–R4 to three parameters: an overall background normalization μ_bkg and two ratios $R(m_\mathrm{T})$ and $R(M_J)$, where the expected background yields are given by $\mu^\mathrm{bkg}_\mathrm{R1} = \mu_\mathrm{bkg}$, $\mu^\mathrm{bkg}_\mathrm{R2} = \mu_\mathrm{bkg} \cdot R(M_J)$, $\mu^\mathrm{bkg}_\mathrm{R3} = \mu_\mathrm{bkg} \cdot R(m_\mathrm{T})$, and $\mu^\mathrm{bkg}_\mathrm{R4} = \kappa \cdot \mu_\mathrm{bkg} \cdot R(M_J) \cdot R(m_\mathrm{T})$.

We perform two types of maximum likelihood fits, which are described in detail in Ref. [12]: (1) a background-only *predictive fit*, which uses the observed yields in R1–R3, assuming no signal contribution, to propagate the uncertainties to μ_bkg, $R(M_J)$, and $R(m_\mathrm{T})$ and (2) a *global fit*, which uses the observed yields in all four regions R1–R4, and allows a non-null signal contribution with known shape but with a floating normalization, yielding a total of four parameters, one for the signal and three for the background. The global fit accounts for signal contamination in R1–R3 and is used to compute signal limits and significances. The predictive fit simplifies theoretical reinterpretation of the results in terms of other models by only requiring comparison of observed and predicted yields in R4 rather than all four regions. In both cases, the likelihood function is written as a product of Poisson terms for the relevant contributions and is performed in bins of $p_\mathrm{T}^\mathrm{miss}$, N_jets, and N_b in R2 and R4, taking into account the correlated yields between the unbinned regions R1 and R3.

Systematic uncertainties in the background prediction are incorporated in the uncertainty in the double-ratio κ. Discrepancies between the value of κ measured in simulation and the true value of κ in the data can in principle arise from mismodeling of the background composition or its properties, including detector effects. These potential discrepancies are estimated using two control samples in data: 5-jet control sample and a dilepton control sample.

To assess the effect of potential mismodeling of the full background composition and its properties, a 5-jet control sample is used. The $N_\mathrm{jets} = 5$ control sample is completely dominated by background processes and has a SM composition very similar to that of the analysis regions.

In particular, this sample probes the rate at which $p_{\mathrm{T}}^{\mathrm{miss}}$ is mismeasured in single-lepton events, increasing the tail of the m_{T} distribution. Such events account for about 7% of the background in the signal region at high $p_{\mathrm{T}}^{\mathrm{miss}}$. This small event category can have a κ value that departs significantly from unity, and it is important to validate the modeling of such effects. Using the analogous R1–R4 regions in the $N_{\mathrm{jets}} = 5$ control sample, κ values are measured in data and are found to be consistent with those obtained from simulation. Because of this consistency, the statistical uncertainty on this comparison in the $N_{\mathrm{jets}} = 5$ control sample is assigned as an uncertainty in κ for each $p_{\mathrm{T}}^{\mathrm{miss}}$ bin of the analysis region. The uncertainties are taken to be fully correlated over the N_{jets} and N_{b} bins.

The dilepton control sample probes potential discrepancies between the κ values in data and simulation as a function of N_{jets}, and it directly probes the dominant background, $\mathrm{t\bar{t}}$ dilepton events. This sample includes not only events with two identified opposite-sign isolated leptons, but also events with one lepton and an oppositely charged veto track. The dilepton control sample in data is substituted for the usual R3 and R4 regions, without an m_{T} requirement, and the quantity κ is measured in bins of N_{jets} and $p_{\mathrm{T}}^{\mathrm{miss}}$. As in the 5-jets control sample, the values of κ measured in data are found to be consistent with those observed in simulation. Because of this consistency, we assign a contribution to the systematic uncertainty in each value of κ used for the actual background predictions that is equal to the statistical uncertainty in this dilepton data-to-simulation comparison. The uncertainties are treated as independent across N_{jets} bins, but are fully correlated across N_{b} and $p_{\mathrm{T}}^{\mathrm{miss}}$ bins. The uncertainties from the dilepton control sample are combined with those from the 5-jet control sample, assuming that the two are uncorrelated.

As a cross-check, we have introduced a broad range of potential effects into simulated event samples to assess their impact on κ. These effects include potential mismodeling of $p_{\mathrm{T}}^{\mathrm{miss}}$ resolution, b-jet tagging efficiencies, initial-state radiation p_{T} and jet-multiplicity distributions, as well as shifts in various background cross sections. These studies show that the impact of plausible mismodeling effects is typically below the few percent level; mismodeling effects large enough to affect κ beyond the systematic uncertainty described above would be evident in the control samples. We therefore take the uncertainty derived from these samples to be sufficient to include all systematic uncertainties in the background estimation.

Systematic uncertainties in the expected signal yield for each model point considered account for mismodeling of the trigger, lepton identification, jet identification, and b-tagging efficiencies in simulated data; mismodeling of the distributions of $p_{\mathrm{T}}^{\mathrm{miss}}$, number of pileup vertices, and ISR jet multiplicity; and uncertainty in the jet energy corrections, QCD scales, and integrated luminosity. The combined effect of all signal-related uncertainties is typically about 25%.

Table 1 lists the observed event yields in region R4 in data, together with the mean background yields from the predictive fit and the expected signal yields from two representative model points. The uncertainties in the predicted background yields include the statistical uncertainties on the event yields in data, the statistical uncertainties on the κ values arising from the finite size of simulated event samples, and the systematic uncertainties on κ as assessed from the data control samples. The observed yields listed in Table 1 are consistent with the background predictions in all of the 18 signal bins to within 2σ, with most of the 18 bins consistent within 1σ. The R4 bins with $p_{\mathrm{T}}^{\mathrm{miss}} > 500$ GeV show an underprediction of the background with respect to the observed yields. However, accounting for the correlations arising from the use of a single, integrated yield in R3 across bins in N_{jets} and N_{b} bins, the statistical significance of the discrepancy in these six bins in R4 is only 1.9σ, mostly due to the bins with $N_{\mathrm{b}} = 1$.

To simplify the reinterpretation of the results in terms of other theoretical models, we provide

Table 1: Observed event yields and mean background yields from the predictive fit in the 18 bins of the signal region R4. The uncertainties in κ include (in order) both a statistical component from the size of the MC samples and a systematic component assessed from data control samples. The uncertainty in the predicted event yield includes both these and the statistical uncertainties associated with the control regions in the data. Also shown are the expected signal yields for two SUSY benchmark models.

Bin in R4	T1tttt (1800,100)	T1tttt (1400,1000)	κ	Pred.	Obs.
$200\ \text{GeV} < p_{\text{T}}^{\text{miss}} \leq 350\ \text{GeV}$					
$6 \leq N_{\text{jets}} \leq 8$, $N_{\text{b}} = 1$	0.4	1.9	$1.2 \pm 0.0 \pm 0.2$	84.6 ± 14.3	106
$6 \leq N_{\text{jets}} \leq 8$, $N_{\text{b}} = 2$	0.6	3.0	$1.2 \pm 0.0 \pm 0.2$	55.1 ± 9.3	75
$6 \leq N_{\text{jets}} \leq 8$, $N_{\text{b}} \geq 3$	0.6	2.2	$1.5 \pm 0.1 \pm 0.2$	16.4 ± 3.0	16
$N_{\text{jets}} \geq 9$, $N_{\text{b}} = 1$	0.2	1.6	$1.0 \pm 0.1 \pm 0.2$	6.5 ± 1.5	11
$N_{\text{jets}} \geq 9$, $N_{\text{b}} = 2$	0.3	2.1	$1.2 \pm 0.1 \pm 0.3$	7.6 ± 1.9	11
$N_{\text{jets}} \geq 9$, $N_{\text{b}} \geq 3$	0.4	3.1	$1.4 \pm 0.1 \pm 0.3$	2.3 ± 0.7	2
$350\ \text{GeV} < p_{\text{T}}^{\text{miss}} \leq 500\ \text{GeV}$					
$6 \leq N_{\text{jets}} \leq 8$, $N_{\text{b}} = 1$	0.7	1.1	$1.0 \pm 0.1 \pm 0.3$	17.4 ± 6.6	25
$6 \leq N_{\text{jets}} \leq 8$, $N_{\text{b}} = 2$	0.9	1.3	$1.1 \pm 0.1 \pm 0.4$	13.7 ± 5.3	10
$6 \leq N_{\text{jets}} \leq 8$, $N_{\text{b}} \geq 3$	0.8	0.9	$1.3 \pm 0.1 \pm 0.4$	3.8 ± 1.6	1
$N_{\text{jets}} \geq 9$, $N_{\text{b}} = 1$	0.3	1.0	$1.1 \pm 0.1 \pm 0.4$	1.3 ± 0.6	2
$N_{\text{jets}} \geq 9$, $N_{\text{b}} = 2$	0.5	1.1	$0.8 \pm 0.1 \pm 0.3$	1.6 ± 0.8	2
$N_{\text{jets}} \geq 9$, $N_{\text{b}} \geq 3$	0.7	2.1	$1.2 \pm 0.2 \pm 0.4$	0.6 ± 0.4	0
$p_{\text{T}}^{\text{miss}} > 500\ \text{GeV}$					
$6 \leq N_{\text{jets}} \leq 8$, $N_{\text{b}} = 1$	2.5	0.6	$1.0 \pm 0.1 \pm 0.3$	1.9 ± 1.5	8
$6 \leq N_{\text{jets}} \leq 8$, $N_{\text{b}} = 2$	3.6	1.0	$1.0 \pm 0.1 \pm 0.3$	0.9 ± 0.7	4
$6 \leq N_{\text{jets}} \leq 8$, $N_{\text{b}} \geq 3$	3.2	0.4	$1.5 \pm 0.3 \pm 0.5$	0.4 ± 0.4	1
$N_{\text{jets}} \geq 9$, $N_{\text{b}} = 1$	1.0	0.7	$1.0 \pm 0.3 \pm 0.4$	0.2 ± 0.2	2
$N_{\text{jets}} \geq 9$, $N_{\text{b}} = 2$	1.8	1.2	$1.0 \pm 0.3 \pm 0.3$	0.1 ± 0.1	0
$N_{\text{jets}} \geq 9$, $N_{\text{b}} \geq 3$	2.3	1.7	$3.1 \pm 1.0 \pm 1.1$	0.1 ± 0.1	0

Table 2: Observed event yields and mean background yields from a predictive fit in four aggregate search bins. In all four cases, the predicted yields refer to R4 with the usual requirements of $m_{\mathrm{T}} > 140$ GeV and $M_J > 400$ GeV applied in addition to the baseline selection. Unlike the finely binned approach, where all 18 background predictions are found simultaneously, the four aggregate bin predictions here are computed separately and may be highly correlated due to overlapping definitions.

Bin	T1tttt (1800,100)	T1tttt (1400,1000)	κ	Pred.	Obs.
$p_{\mathrm{T}}^{\mathrm{miss}} > 200$ GeV, $N_{\mathrm{jets}} \geq 9$, $N_{\mathrm{b}} \geq 3$	3.4	6.9	1.4 ± 0.3	3.1 ± 0.8	2
$p_{\mathrm{T}}^{\mathrm{miss}} > 350$ GeV, $N_{\mathrm{jets}} \geq 9$, $N_{\mathrm{b}} \geq 2$	5.3	6.2	1.0 ± 0.4	2.7 ± 1.2	2
$p_{\mathrm{T}}^{\mathrm{miss}} > 500$ GeV, $N_{\mathrm{jets}} \geq 6$, $N_{\mathrm{b}} \geq 3$	5.4	2.1	1.7 ± 0.6	0.5 ± 0.4	1
$p_{\mathrm{T}}^{\mathrm{miss}} > 500$ GeV, $N_{\mathrm{jets}} \geq 9$, $N_{\mathrm{b}} \geq 1$	5.1	3.6	1.2 ± 0.4	0.4 ± 0.4	2

predicted mean background yields for four aggregated search bins, shown in Table 2. The aggregate bins are defined such that at least one bin will provide sensitivity to most of the models for which the finely binned analysis has sensitivity. Since the aggregate bins overlap, they are intended to be used one at a time, unlike the 18 non-overlapping signal bins, which are considered simultaneously in one fit. The choice of the best aggregate bin will depend on the properties of the model under consideration. Each prediction includes all sources of uncertainty.

Figure 1 compares the shapes of the M_J distributions observed in data in the single-lepton sample for $m_{\mathrm{T}} \leq 140$ GeV and $m_{\mathrm{T}} > 140$ GeV. The baseline selection, together with the requirements $N_{\mathrm{b}} \geq 2$ and either $200 < p_{\mathrm{T}}^{\mathrm{miss}} \leq 350$ GeV or $p_{\mathrm{T}}^{\mathrm{miss}} > 350$ GeV, are applied. In the absence of signal, the shapes of the distributions at low and high m_{T} should be consistent, as observed. The lower $p_{\mathrm{T}}^{\mathrm{miss}}$ region shows the background behavior with higher statistics, while the higher $p_{\mathrm{T}}^{\mathrm{miss}}$ region has higher sensitivity to the signal.

An interpretation of the results in the T1tttt mass plane is shown in Fig. 2 (left). Cross section upper limits at a 95% confidence level are shown by the color map as a function of $m_{\tilde{g}}$ and $m_{\tilde{\chi}_1^0}$. Model points below the black curve have a theoretical cross section above the observed upper limit and are excluded by this analysis. Expected limits are computed using the background-only hypothesis, with nuisance parameters assuming their best-fit values from the observed data. Figure 2 (right) shows the expected and observed limits for both T1tttt and T5tttt, where in T5tttt it is assumed that the top squark mass is 175 GeV above the neutralino mass, a limiting case in terms of sensitivity to the decay kinematics. For most of the excluded region, the boundaries for T1tttt and T5tttt are very similar, indicating only a weak overall sensitivity to the value of the top squark mass. At low values of $m(\tilde{\chi}_1^0)$ in T5tttt, the sensitivity is reduced because the neutralino carries very little momentum; however, some sensitivity is provided by dilepton events that escape the lepton veto [12].

In summary, we have performed a search for an excess event yield above that expected for SM processes using a data sample of proton-proton collision events with an integrated luminosity of 35.9 fb^{-1} at $\sqrt{s} = 13$ TeV. The signature is based on events with large missing transverse momentum, a single isolated lepton, multiple high p_{T} jets, and at least one b-tagged jet. No significant excesses above the expected SM backgrounds is observed in any of the signal regions. The results are interpreted in the framework of simplified models that describe important natural SUSY scenarios with gluino pair production, followed by gluino decay into top quarks and a neutralino. For three-body decay, gluinos with masses below 1.9 TeV are excluded at a 95% CL for neutralino masses up to about 1 TeV. The results for two-body gluino decay are

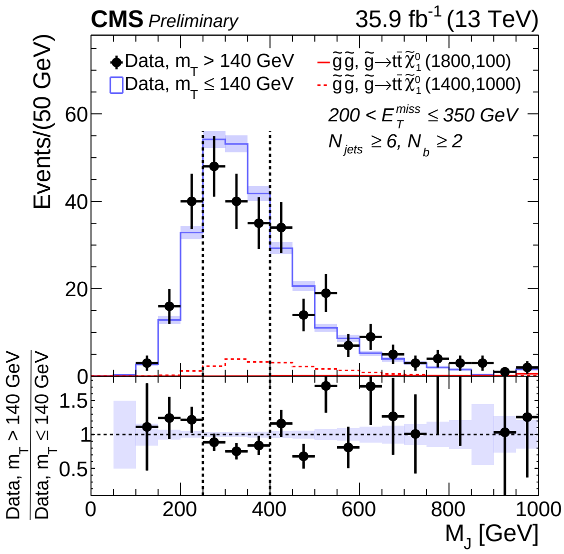

Figure 1: Distributions of M_J observed in data for $200 < p_{\mathrm{T}}^{\mathrm{miss}} \leq 350$ GeV (left) and $p_{\mathrm{T}}^{\mathrm{miss}} > 350$ GeV (right) in the 1ℓ data for low (≤ 140 GeV) m_{T} and high (> 140 GeV) m_{T} regions. In each plot, the data at low m_{T} have been renormalized to the yield observed at high m_{T} to facilitate the comparison of the shapes of the distributions. The vertical dashed line at $M_J = 250$ GeV shows the lower boundary of regions R1 and R3, while the vertical line at $M_J = 400$ GeV separates R1 and R3 from R2 and R4. The data are integrated over $N_{\mathrm{jets}} \geq 6$ and $N_{\mathrm{b}} \geq 2$. Two SUSY benchmark models are shown in the solid and dashed red histograms.

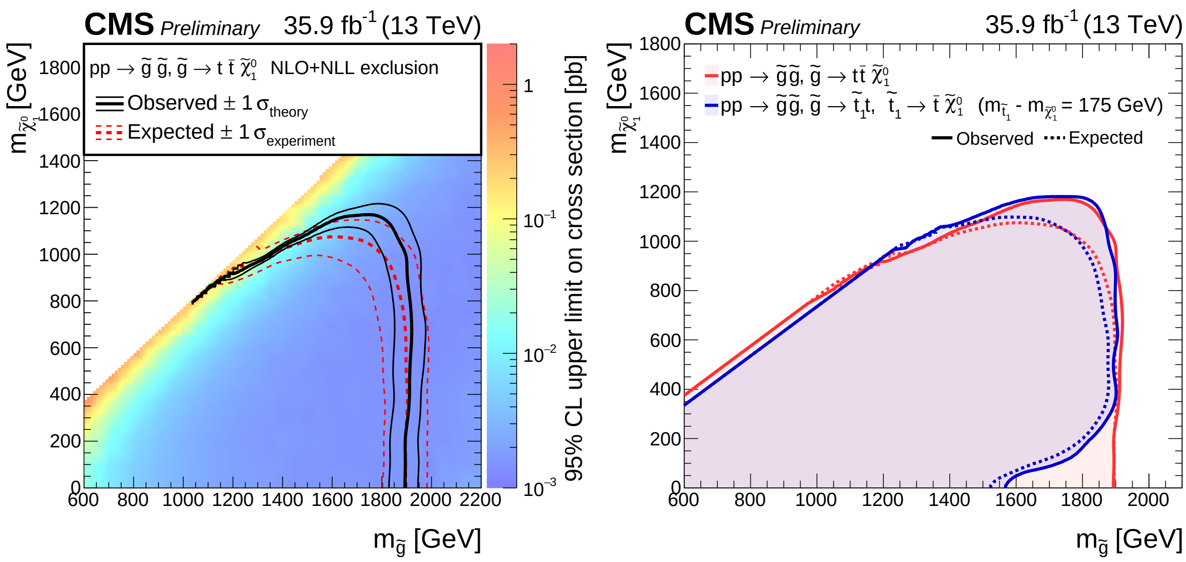

Figure 2: Left: excluded cross sections and SUSY particle masses for the T1tttt model. The color map indicates cross section time branching fraction upper limits at a 95% confidence level across the T1tttt mass plane. The black (red) line shows the observed (expected) exclusion of mass scenarios with theoretical cross sections higher than their respective upper limits. Limits are computed using the global fit. Right: comparison of the excluded gluino and LSP masses for the T1tttt and T5tttt models. The gluino mass limits are similar except at low $m_{\tilde{\chi}_1^0}$.

generally similar except at low neutralino masses, where the exclusion weakens. These results are among the most stringent constraints on these SUSY models to date.

References

[1] P. Ramond, "Dual theory for free fermions", *Phys. Rev. D* **3** (1971) 2415, doi:10.1103/PhysRevD.3.2415.

[2] Y. A. Golfand and E. P. Likhtman, "Extension of the algebra of Poincaré group generators and violation of P invariance", *JETP Lett.* **13** (1971) 323.

[3] A. Neveu and J. H. Schwarz, "Factorizable dual model of pions", *Nucl. Phys. B* **31** (1971) 86, doi:10.1016/0550-3213(71)90448-2.

[4] D. V. Volkov and V. P. Akulov, "Possible universal neutrino interaction", *JETP Lett.* **16** (1972) 438.

[5] J. Wess and B. Zumino, "A Lagrangian model invariant under supergauge transformations", *Phys. Lett. B* **49** (1974) 52, doi:10.1016/0370-2693(74)90578-4.

[6] J. Wess and B. Zumino, "Supergauge transformations in four dimensions", *Nucl. Phys. B* **70** (1974) 39, doi:10.1016/0550-3213(74)90355-1.

[7] P. Fayet, "Supergauge invariant extension of the Higgs mechanism and a model for the electron and its neutrino", *Nucl. Phys. B* **90** (1975) 104, doi:10.1016/0550-3213(75)90636-7.

[8] H. P. Nilles, "Supersymmetry, supergravity and particle physics", *Phys. Rep.* **110** (1984) 1, doi:10.1016/0370-1573(84)90008-5.

[9] ATLAS Collaboration, "Search for squarks and gluinos in events with isolated leptons, jets and missing transverse momentum at $\sqrt{s} = 8$ TeV with the ATLAS detector", *JHEP* **04** (2015) 116, doi:10.1007/JHEP04(2015)116, arXiv:1501.03555.

[10] CMS Collaboration, "Search for supersymmetry in pp collisions at $\sqrt{s} = 8$ TeV in events with a single lepton, large jet multiplicity, and multiple b jets", *Phys. Lett. B* **733** (2014) 328, doi:10.1016/j.physletb.2014.04.023, arXiv:1311.4937.

[11] ATLAS Collaboration, "Search for gluinos in events with an isolated lepton, jets and missing transverse momentum at $\sqrt{s} = 13$ TeV with the ATLAS detector", *Eur. Phys. J. C* **76** (2016), no. 10, 565, doi:10.1140/epjc/s10052-016-4397-x, arXiv:1605.04285.

[12] CMS Collaboration, "Search for supersymmetry in pp collisions at $\sqrt{s} = 13$ TeV in the single-lepton final state using the sum of masses of large-radius jets", *JHEP* **08** (2016) 122, doi:10.1007/JHEP08(2016)122, arXiv:1605.04608.

[13] CMS Collaboration, "Search for supersymmetry in events with one lepton and multiple jets in proton-proton collisions at $\sqrt{s} = 13$ TeV", *Phys. Rev. D* **95** (2017) 012011, doi:10.1103/PhysRevD.95.012011, arXiv:1609.09386.

[14] ATLAS Collaboration, "Observation of a new particle in the search for the Standard Model Higgs boson with the ATLAS detector at the LHC", *Phys. Lett. B* **716** (2012) 1, doi:10.1016/j.physletb.2012.08.020, arXiv:1207.7214.

[15] CMS Collaboration, "Observation of a new boson at a mass of 125 GeV with the CMS experiment at the LHC", *Phys. Lett. B* **716** (2012) 30, doi:10.1016/j.physletb.2012.08.021, arXiv:1207.7235.

[16] CMS Collaboration, "Observation of a new boson with mass near 125 GeV in pp collisions at $\sqrt{s}$ = 7 and 8 TeV", *JHEP* **06** (2013) 081, doi:10.1007/JHEP06(2013)081, arXiv:1303.4571.

[17] CMS Collaboration, "Precise determination of the mass of the Higgs boson and tests of compatibility of its couplings with the standard model predictions using proton collisions at 7 and 8 TeV", *Eur. Phys. J. C* **75** (2015) 212, doi:10.1140/epjc/s10052-015-3351-7, arXiv:1412.8662.

[18] ATLAS Collaboration, "Measurement of the Higgs boson mass from the $\mathrm{H} \to \gamma\gamma$ and $\mathrm{H} \to \mathrm{ZZ}^* \to 4\ell$ channels with the ATLAS detector using 25 fb^{-1} of pp collision data", *Phys. Rev. D* **90** (2014) 052004, doi:10.1103/PhysRevD.90.052004, arXiv:1406.3827.

[19] ATLAS and CMS Collaborations, "Combined Measurement of the Higgs Boson Mass in pp Collisions at $\sqrt{s} = 7$ and 8 TeV with the ATLAS and CMS Experiments", *Phys. Rev. Lett.* **114** (2015) 191803, doi:10.1103/PhysRevLett.114.191803, arXiv:1503.07589.

[20] G. 't Hooft, "Naturalness, chiral symmetry, and spontaneous chiral symmetry breaking", *NATO Sci. Ser. B* **59** (1980) 135.

[21] E. Witten, "Dynamical Breaking of Supersymmetry", *Nucl. Phys. B* **188** (1981) 513, doi:10.1016/0550-3213(81)90006-7.

[22] M. Dine, W. Fischler, and M. Srednicki, "Supersymmetric Technicolor", *Nucl. Phys. B* **189** (1981) 575, doi:10.1016/0550-3213(81)90582-4.

[23] S. Dimopoulos and S. Raby, "Supercolor", *Nucl. Phys. B* **192** (1981) 353, doi:10.1016/0550-3213(81)90430-2.

[24] S. Dimopoulos and H. Georgi, "Softly Broken Supersymmetry and SU(5)", *Nucl. Phys. B* **193** (1981) 150, doi:10.1016/0550-3213(81)90522-8.

[25] R. K. Kaul and P. Majumdar, "Cancellation of Quadratically Divergent Mass Corrections in Globally Supersymmetric Spontaneously Broken Gauge Theories", *Nucl. Phys. B* **199** (1982) 36, doi:10.1016/0550-3213(82)90565-X.

[26] S. Dimopoulos and G. F. Giudice, "Naturalness constraints in supersymmetric theories with nonuniversal soft terms", *Phys. Lett. B* **357** (1995) 573, doi:10.1016/0370-2693(95)00961-J, arXiv:hep-ph/9507282.

[27] R. Barbieri and D. Pappadopulo, "S-particles at their naturalness limits", *JHEP* **10** (2009) 061, doi:10.1088/1126-6708/2009/10/061, arXiv:0906.4546.

[28] M. Papucci, J. T. Ruderman, and A. Weiler, "Natural SUSY endures", *JHEP* **09** (2012) 035, doi:10.1007/JHEP09(2012)035, arXiv:1110.6926.

[29] J. L. Feng, "Naturalness and the Status of Supersymmetry", *Ann. Rev. Nucl. Part. Sci.* **63** (2013) 351, doi:10.1146/annurev-nucl-102010-130447, arXiv:1302.6587.

[30] G. R. Farrar and P. Fayet, "Phenomenology of the Production, Decay, and Detection of New Hadronic States Associated with Supersymmetry", *Phys. Lett. B* **76** (1978) 575, doi:10.1016/0370-2693(78)90858-4.

[31] S. P. Martin, "A supersymmetry primer", *Adv. Ser. Direct. High Energy Phys.* **18** (1998) 1, doi:10.1142/9789812839657_0001, arXiv:hep-ph/9709356.

[32] CMS Collaboration, "Interpretation of Searches for Supersymmetry with simplified Models", *Phys. Rev. D* **88** (2013) 052017, doi:10.1103/PhysRevD.88.052017, arXiv:1301.2175.

[33] J. Alwall, P. Schuster, and N. Toro, "Simplified models for a first characterization of new physics at the LHC", *Phys. Rev. D* **79** (2009) 075020, doi:10.1103/PhysRevD.79.075020, arXiv:0810.3921.

[34] J. Alwall, M.-P. Le, M. Lisanti, and J. G. Wacker, "Model-independent jets plus missing energy searches", *Phys. Rev. D* **79** (2009) 015005, doi:10.1103/PhysRevD.79.015005, arXiv:0809.3264.

[35] D. Alves et al., "Simplified models for LHC new physics searches", *J. Phys. G* **39** (2012) 105005, doi:10.1088/0954-3899/39/10/105005, arXiv:1105.2838.

[36] CMS Collaboration, "The CMS experiment at the CERN LHC", *JINST* **3** (2008) S08004, doi:10.1088/1748-0221/3/08/S08004.

[37] J. Alwall et al., "The automated computation of tree-level and next-to-leading order differential cross sections, and their matching to parton shower simulations", *JHEP* **07** (2014) 079, doi:10.1007/JHEP07(2014)079, arXiv:1405.0301.

[38] GEANT4 Collaboration, "GEANT4 — a simulation toolkit", *Nucl. Instrum. Meth. A* **506** (2003) 250, doi:10.1016/S0168-9002(03)01368-8.

[39] CMS Collaboration, "The fast simulation of the CMS detector at LHC", *J. Phys. Conf. Ser.* **331** (2011) 032049, doi:10.1088/1742-6596/331/3/032049.

[40] CMS Collaboration, "Particle flow event reconstruction in CMS and performance for jets, taus and $E_{\mathrm{T}}^{\mathrm{miss}}$", CMS Physics Analysis Summary CMS-PAS-PFT-09-001, CERN, 2009.

[41] CMS Collaboration, "Commissioning of the particle-flow event reconstruction with the first LHC collisions recorded in the CMS detector", CMS Physics Analysis Summary CMS-PAS-PFT-10-001, CERN, 2010.

[42] CMS Collaboration, "Performance of electron reconstruction and selection with the CMS detector in proton-proton collisions at $\sqrt{s} = 8$ TeV", *JINST* **10** (2015) P06005, doi:10.1088/1748-0221/10/06/P06005, arXiv:1502.02701.

[43] CMS Collaboration, "Performance of CMS muon reconstruction in pp collision events at $\sqrt{s} = 7$ TeV", *JINST* **7** (2012) P10002, doi:10.1088/1748-0221/7/10/P10002, arXiv:1206.4071.

[44] K. Rehermann and B. Tweedie, "Efficient Identification of Boosted Semileptonic Top Quarks at the LHC", *JHEP* **03** (2011) 059, doi:10.1007/JHEP03(2011)059, arXiv:1007.2221.

[45] C. Lester and D. Summers, "Measuring masses of semi-invisibly decaying particle pairs produced at hadron colliders", *Phys. Lett. B* **463** (1999) 5, doi:10.1016/S0370-2693(99)00945-4.

[46] M. Cacciari, G. P. Salam, and G. Soyez, "The anti-k_t jet clustering algorithm", *JHEP* **04** (2008) 063, doi:10.1088/1126-6708/2008/04/063, arXiv:0802.1189.

[47] M. Cacciari, G. P. Salam, and G. Soyez, "FastJet User Manual", *Eur. Phys. J.* **C72** (2012) 1896, doi:10.1140/epjc/s10052-012-1896-2, arXiv:1111.6097.

[48] CMS Collaboration, "Identification of b-quark jets with the CMS experiment", *JINST* **8** (2013) P04013, doi:10.1088/1748-0221/8/04/P04013, arXiv:1211.4462.

[49] CMS Collaboration, "Identification of b quark jets at the CMS Experiment in the LHC Run 2", CMS Physics Analysis Summary CMS-PAS-BTV-15-001, CERN, 2016.